Molecular Analysis of the Interaction Between Staphylococcal Virulence Factor Sbi-IV and Complement C3d

Supporting Material

12 figures, 1 table, and 3 movies (available online)

Ronald D. Gorham Jr., Wilson Rodriguez, and Dimitrios Morikis
Department of Bioengineering, University of California, Riverside, CA 92521

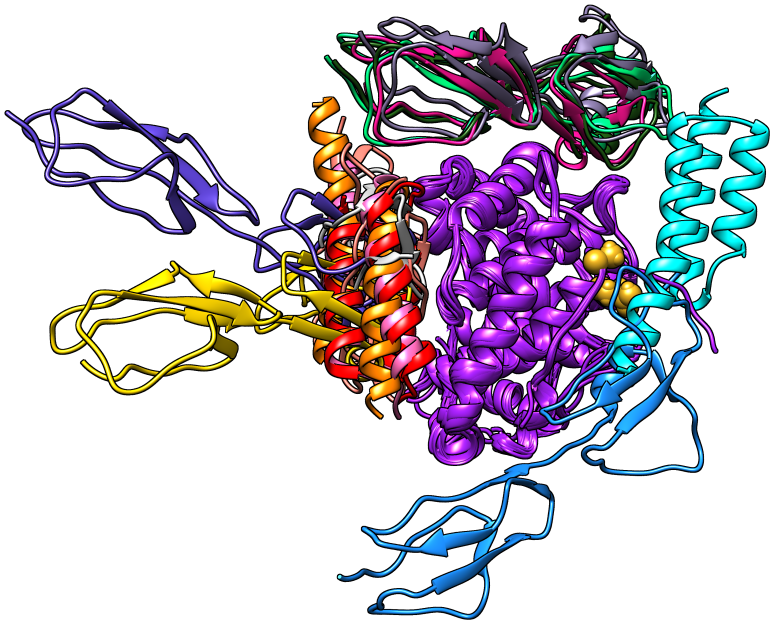

FIGURE S1. Structures of known ligands in complex with C3d. This figure shows a ribbon representation of C3d (purple) in complex with Sbi-IV (Complex 1, orange; Complex 2, cyan, (1)), Efb-C (pink, (2)), Ecb (red, (3)), CR2 (salmon, (4)), Factor H Domains 19-20 (Morgan et al. Chain A-D, blue (5); Morgan et al. Chain A-E, green (5); Morgan et al. Chain B-D, indigo (5); Morgan et al. Chain B-F, dark green (5); Morgan et al. Chain C-D, light purple (5); Kajander et al. Chain A-C, magenta (6); Kajander et al. Chain B-C, yellow (6)), and Factor H Domain 4 (light gray, (7)). The location of the thioester bond in the convex surface of C3d is shown as gold spheres. The location of the thioester bond in the convex surface of C3d is shown as gold spheres. The location of the concave surface of C3d is located at the opposite site of the convex surface.

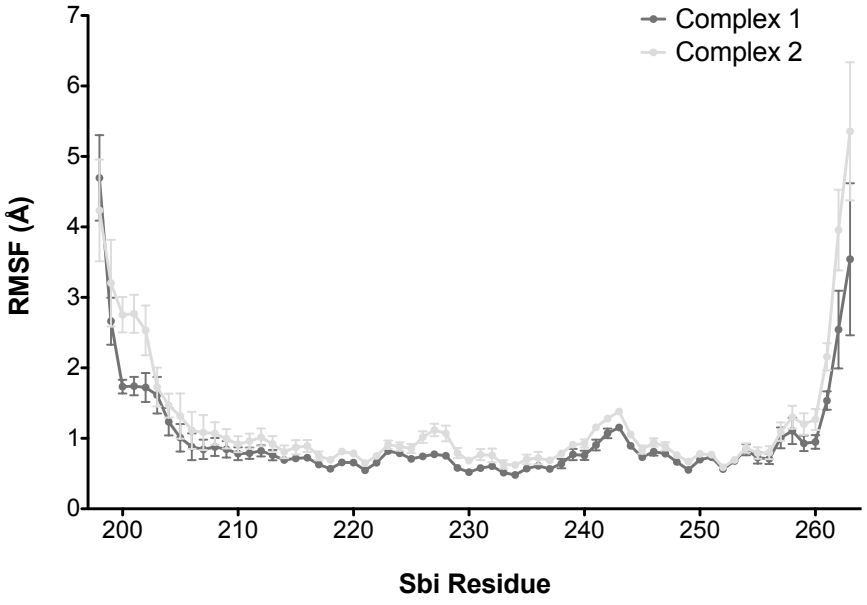

FIGURE S2. Root mean square fluctuation of Sbi-IV residues in Complex 1 (dark gray) and Complex 2 (light gray). Values represent mean +/- SD over four independent trajectories.

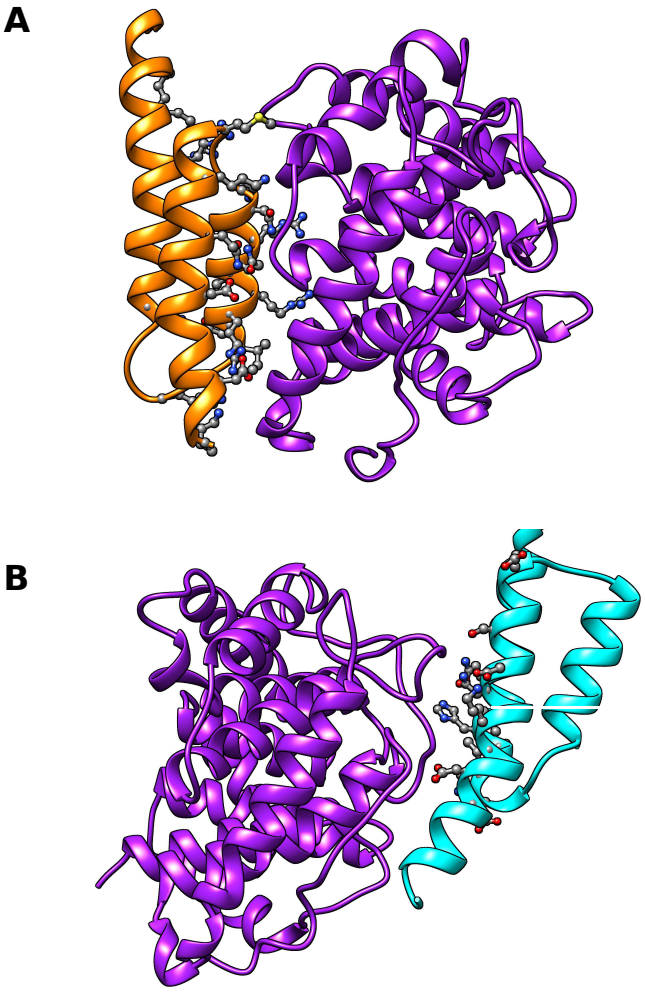

FIGURE S3. Distribution of C3d-Sbi-IV interactions in Complex 1 and 2. (A) Crystallographic structure of Complex 1, with C3d colored in purple and Sbi-IV colored in orange. (B) Crystallographic structure of Complex 2, with C3d colored in purple and Sbi-IV colored in cyan. Sbi-IV residues that interact with C3d (with significant energetic contributions) are shown in ball-and-stick representation.

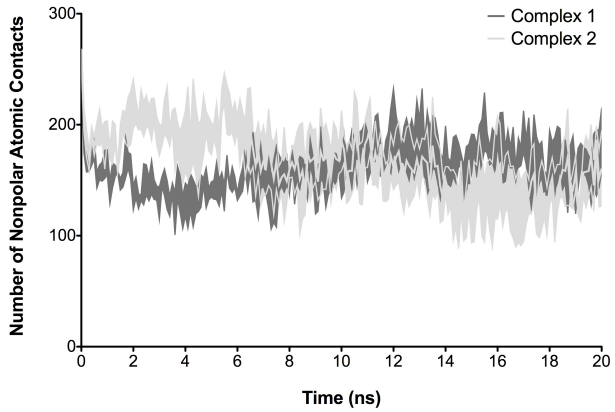

FIGURE S4. Number of nonpolar atomic contacts during MD trajectories. The plot shows the mean +/- SEM of the number of nonpolar atomic contacts in Complex 1 (dark gray) and Complex 2 (light gray) of C3d-Sbi-IV during three independent 20 ns MD trajectories.

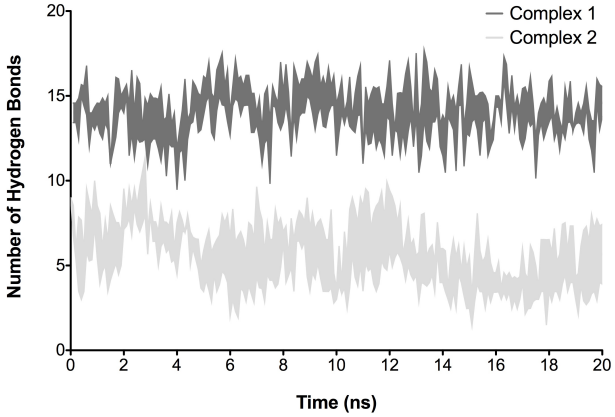

FIGURE S5. Number of hydrogen bonds during MD trajectories. The plot shows the mean +/- SEM of the number of hydrogen bonds in Complex 1 (dark gray) and Complex 2 (light gray) of C3d-Sbi-IV during three independent 20 ns MD trajectories.

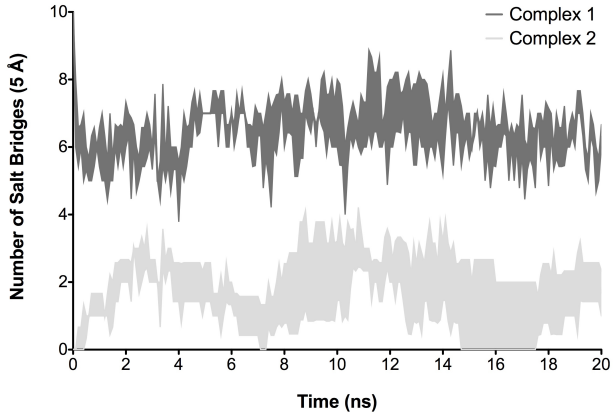

FIGURE S6. Number of salt bridges (measured as charge-charge distance of < 5 Å) during MD trajectories. The plot shows the mean +/- SEM of the number of hydrogen bonds in Complex 1 (dark gray) and Complex 2 (light gray) of C3d-Sbi-IV during three independent 20 ns MD trajectories.

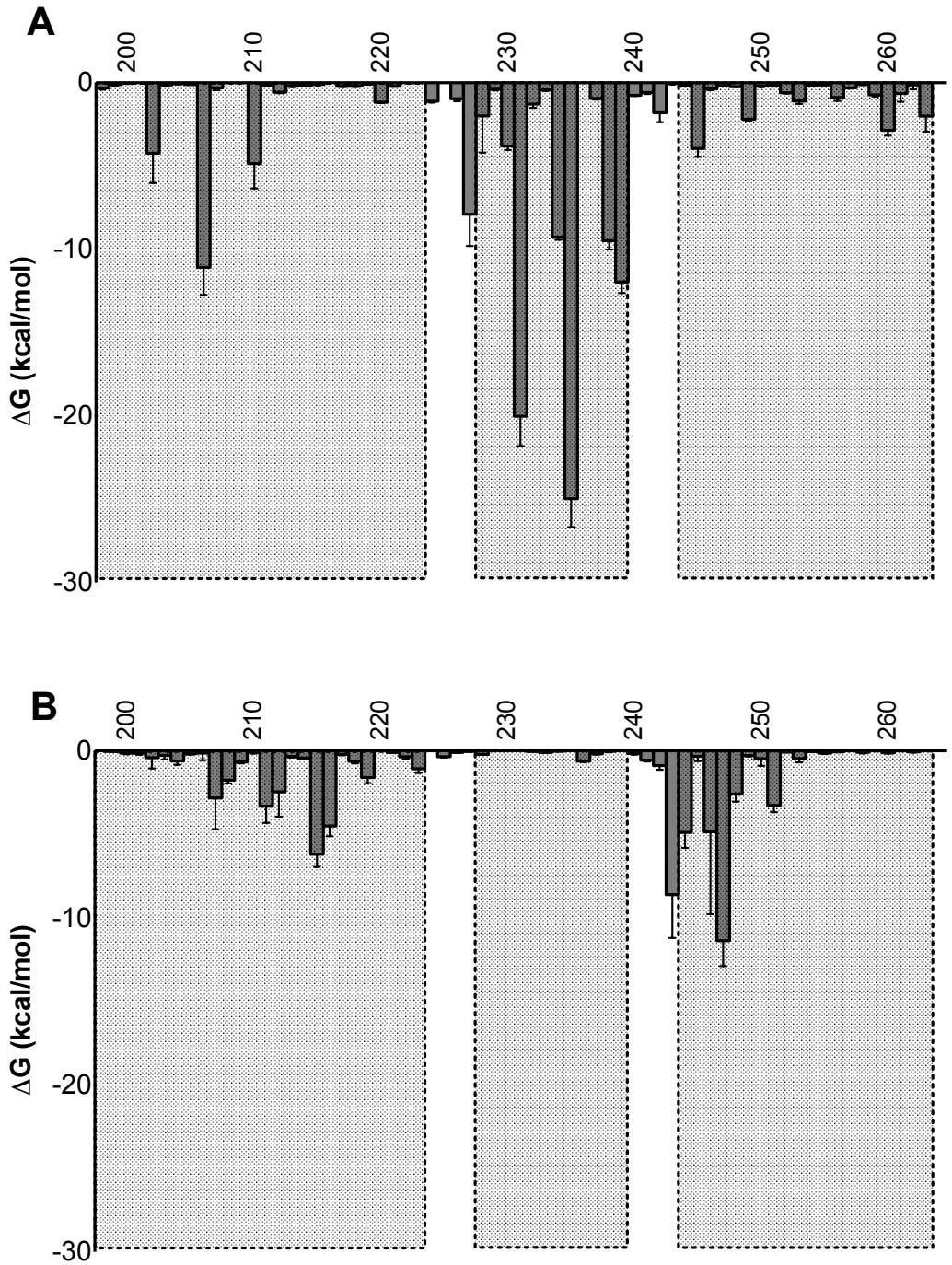

FIGURE S7. Per-residue MM-GBSA free energies for Sbi-IV in Complex 1 (A) and Complex 2 (B). All Sbi-IV residues are shown. The three vertical shaded boxes represent residue ranges of helix 1, 2, and 3 of Sbi-IV.

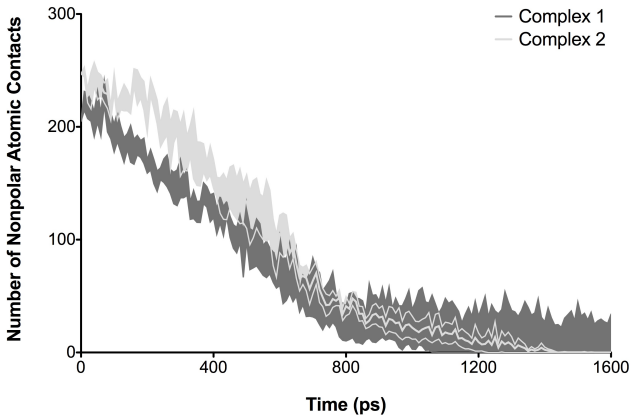

FIGURE S8. Number of nonpolar atomic contacts during SMD trajectories. The plot shows the mean +/- SEM of the number of nonpolar atomic contacts in Complex 1 (dark gray) and Complex 2 (light gray) of C3d-Sbi-IV during five independent 1.6 ns SMD trajectories.

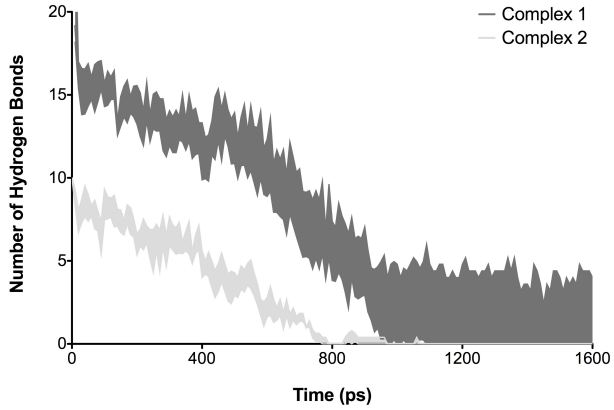

FIGURE S9. Number of hydrogen bonds during SMD trajectories. The plot shows the mean +/- SEM of the number of hydrogen bonds in Complex 1 (dark gray) and Complex 2 (light gray) of C3d-Sbi-IV during five independent 1.6 ns SMD trajectories.

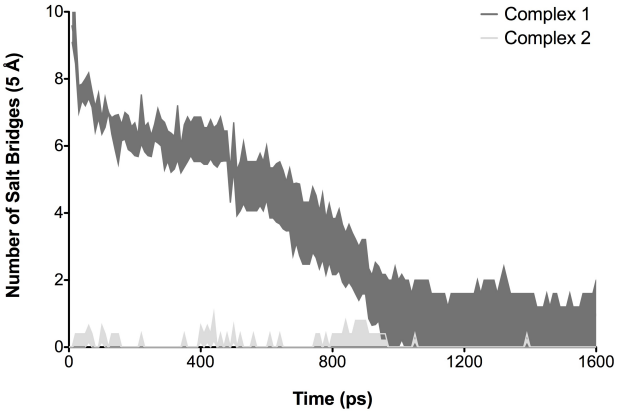

FIGURE S10. Number of salt bridges (measured as charge-charge distance of < 5 Å) during SMD trajectories. The plot shows the mean +/- SEM of the number of hydrogen bonds in Complex 1 (dark gray) and Complex 2 (light gray) of C3d-Sbi-IV during five independent 1.6 ns SMD trajectories.

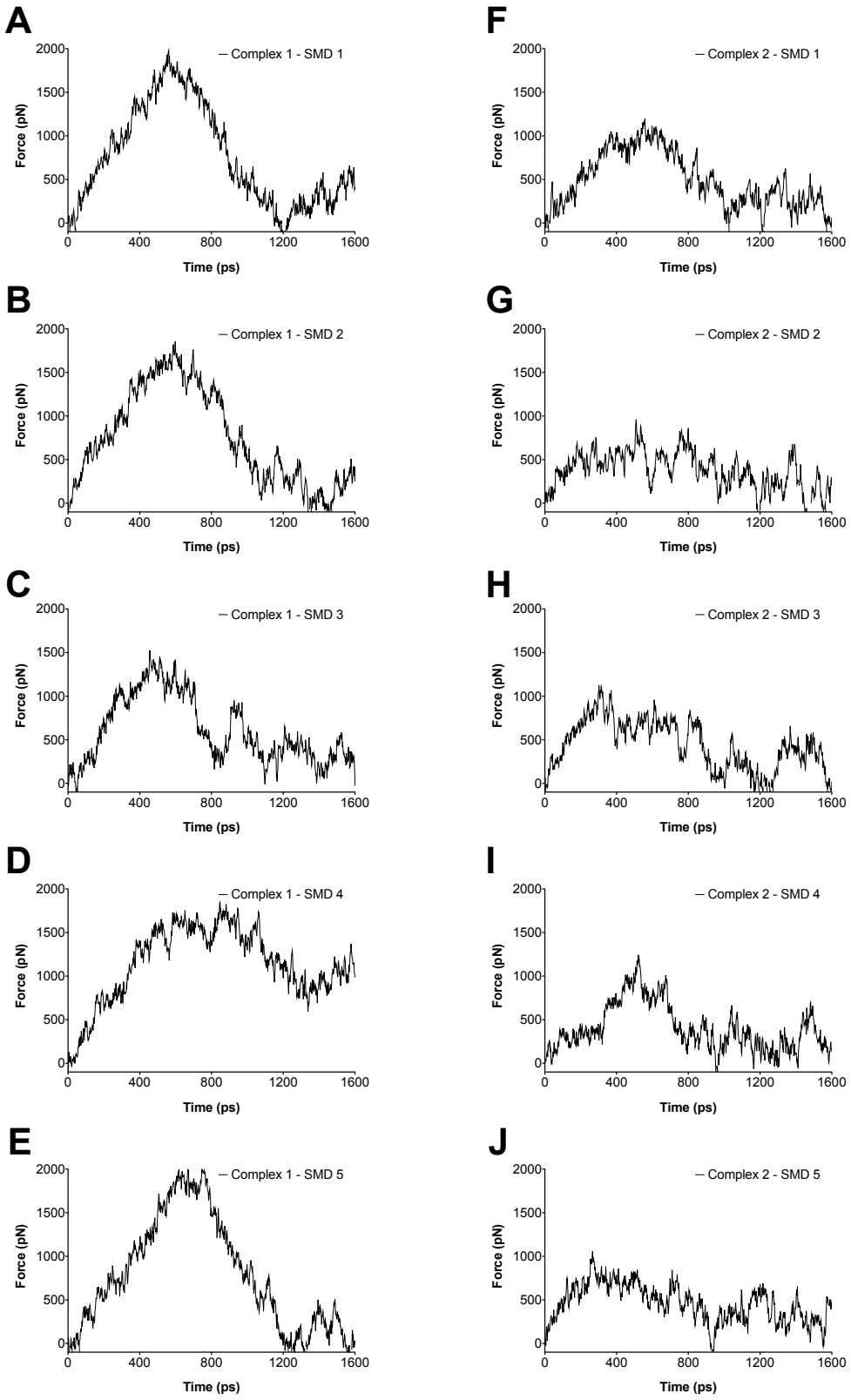

FIGURE S11. Force-time plots from SMD simulations. Panels A-E represent simulations of Complex 1, and panels F-J represent simulations from Complex 2.

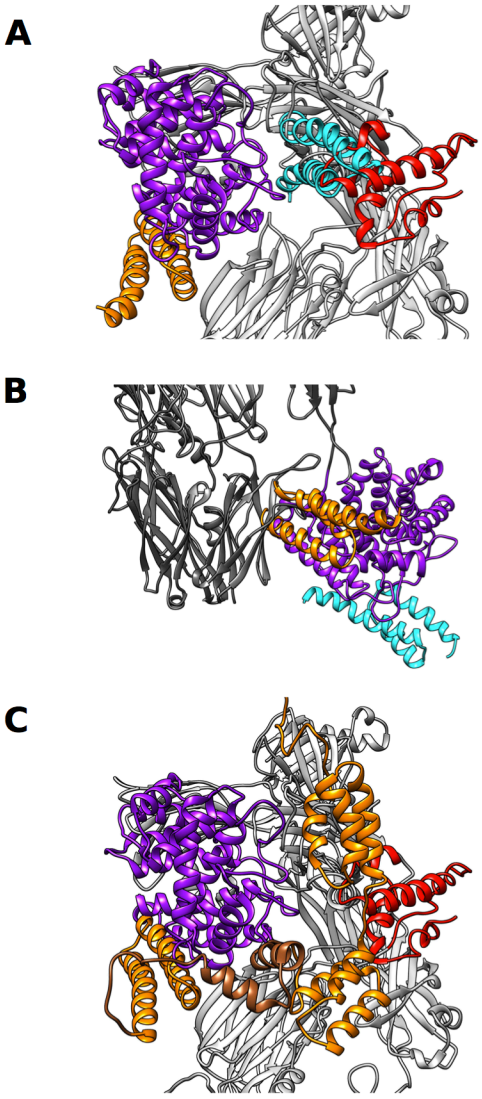

FIGURE S12. Sbi binding to C3 and C3b. (A) Ribbon representation of Sbi-IV bound to C3 (gray) in Complex 1 (orange) and Complex 2 (cyan) binding modes. The thioester domain of C3 (C3d) is colored in purple, and the anaphylotoxin domain (C3a) is colored in red. Steric clashes exist between Sbi-IV of Complex 2 and the anaphylotoxin and MG8 domains of C3. (B) Sbi-IV binding to C3b (dark gray). Steric clashes exist between Sbi-IV of Complex 1 and MG1 domain of C3b. (C) Model of full-length extracellular Sbi (domains I-IV) bound to C3, with Sbi-IV bound in the Complex 1 binding mode. Sbi is colored in orange, with domain III colored in brown. Note the flexible loop region between domains III and IV, and the potential of domain III to reach C3a (in red).

MOVIE CAPTIONS

MOVIE S1. MD simulations of C3d-Sbi-IV complexes. Coordinates from C3d in both complexes were superimposed (purple ribbon), and Sbi-IV in Complex 1 and 2 binding modes are shown in orange (left) and cyan (right), respectively. Note the flexibility of the N-terminus of Sbi-IV in the Complex 2 binding mode (bottom right, terminus of cyan ribbon). The N-terminus moves away from C3d over the course of the simulation. The movie shows representative simulations (20 ns) for each complex binding mode.

MOVIE S2. BD simulation of C3d-Sbi-IV complex. This movie shows an example of a successful Sbi-IV association trajectory with C3d in the Complex 1 binding mode. C3d (stationary, left) is shown as a purple ribbon, and Sbi-IV (diffusing, right) is shown as a cyan ribbon. Note the rapid encounter of C3d and Sbi-IV, followed by localized diffusion to form specific charge-charge interactions between basic Sbi-IV residues (blue spheres) and acidic C3d residues (red spheres).

MOVIE S3. SMD simulations of C3d-Sbi-IV complexes. Coordinates from C3d in both complexes were superimposed (purple ribbon), and Sbi-IV in Complex 1 and 2 binding modes are shown in orange (left) and cyan (right), respectively. Sbi-IV residues involved in intermolecular C3d-Sbi-IV interactions are shown as gray sticks. Sbi-IV molecules are pulled at constant velocity in a direction perpendicular to their respective binding interfaces. Note the larger number and dispersion of interactions in Complex 1 compared to Complex 2.

Table S1. C3d-Sbi-IV interactions from MD snapshots.

	Complex 1		Complex 2	
	Nonpolar	H-bonds	Nonpolar	H-bonds
0 ns	D225, I227, R230, R231, Q234, R235, N238, M242, K245, Q249, V256, D260, K263	**R206-E1160** **R231-D1029** **R235-D1156** N238-S1097 **K239-D1156** K245-I1095	I200, E201, I204, V205, H207, D208, V211, K212, N215, D216, S219, V244, H247, L248	I204-Q1013 D208-A1010 D208-Q1013 N215-K1071 N215-K1072 S219-K1071 D243-Y1266 Q251-R1072
25 ns	R206 ,R210, I227, R231, Q234, R235, N238, K239, M242, K245, Q249	**K202-E1160** **R206-E1159** **R206-E1160** **R231-D1029** **R231-E1030** R235-N1091 **R235-D1156** N238-V1090 N238-I1093 N238-I1095 **K239-D1156** K245-I1095	H207, V211, D243, V244, H247, L248	Q251-R1072
50 ns	H207, R210, R231, Q234, R235, N238, K239, M242, K245, Q249, D260, A261	**R206-E1160** **R231-D1029** **R231-E1030** **R235-D1156** N238-V1090 N238-I1093 N238-I1095 **K239-D1156** K245-I1095 A261-Q1043	V211, N215, D243, V244, H247, L248	N215-K1071 D243-Q1127 H247-R1072 Q251-R1072
75 ns	R210, I227, R231, Q234, R235, N238, K239, Q249	**K202-E1160** **R206-E1159** **R206-E1160** **R231-E1030** R235-N1091 **R235-D1156** N238-V1090 N238-I1093 **K239-D1156** K245-S1097	H207, V211, N215, D216, S219, D243, V244, E246, H247, L248	N215-K1071 **D216-K1071** D243-Q1127 H247-R1072 Q251-R1072
100 ns	R206, R210, I227, R231, Q234, R235, N238, K239, K245, Q249, D260	**R206-E1160** **E228-K1284** **R231-E1030** R235-N1091 **R235-D1156** N238-V1090 N238-I1093 N238-S1097 **K239-D1156** **K245-D1096**	H207, V211, K212, N215, D216, S219, D243, V244, H247, L248	K202-Q1013 H207-A1010 D243-Q1127 D243-Y1266 H247-R1072 Q251-R1072

***** Interactions are for Complex 1 and 2, at snapshots as shown in Figure 3. The "Nonpolar" columns show Sbi-IV residues involved in intermolecular van der Waals interactions. The "H-bonds" sections show intermolecular hydrogen bonds, with salt bridges (< 5Å distance) highlighted in bold. The 0 ns snapshots represent the unaltered crystallographic structures.

SUPPORTING REFERENCES

1. Clark, E.A., S. Crennell, A. Upadhyay, A.V. Zozulya, J.D. Mackay, D.I. Svergun, S. Bagby, and J.M.H. van den Elsen. 2010. A structural basis for Staphylococcal complement subversion: X-ray structure of the complement-binding domain of *Staphylococcus aureus* protein Sbi in complex with ligand C3d. *Mol. Immunol.* 48: 452–462.

2. Hammel, M., G. Sfyroera, D. Ricklin, P. Magotti, J.D. Lambris, and B.V. Geisbrecht. 2007. A structural basis for complement inhibition by *Staphylococcus aureus*. *Nat. Immunol.* 8: 430–437.

3. Hammel, M., G. Sfyroera, S. Pyrpassopoulos, D. Ricklin, K.X. Ramyar, M. Pop, Z. Jin, J.D. Lambris, and B.V. Geisbrecht. 2007. Characterization of Ehp, a secreted complement inhibitory protein from *Staphylococcus aureus*. *J. Biol. Chem.* 282: 30051–30061.

4. van den Elsen, J.M.H., and D.E. Isenman. 2011. Complement receptor complex structure. *Science*. 332: 608–611.

5. Morgan, H.P., C.Q. Schmidt, M. Guariento, B.S. Blaum, D. Gillespie, A.P. Herbert, D. Kavanagh, H.D.T. Mertens, D.I. Svergun, C.M. Johansson, D. Uhrín, P.N. Barlow, and J.P. Hannan. 2011. Structural basis for engagement by complement factor H of C3b on a self surface. *Nat. Struct. Mol. Biol.* 18: 463–470.

6. Kajander, T., M.J. Lehtinen, S. Hyvärinen, A. Bhattacharjee, E. Leung, D.E. Isenman, S. Meri, A. Goldman, and T.S. Jokiranta. 2011. Dual interaction of factor H with C3d and glycosaminoglycans in host-nonhost discrimination by complement. *Proc. Natl. Acad. Sci. U.S.A.* 108: 2897–2902.

7. Wu, J., Y.-Q. Wu, D. Ricklin, B.J.C. Janssen, J.D. Lambris, and P. Gros. 2009. Structure of complement fragment C3b–factor H and implications for host protection by complement regulators. *Nat. Immunol*. 10: 729–734.